PERGAMON

International Journal of Solids and Structures 40 (2003) 6497–6512

INTERNATIONAL JOURNAL OF SOLIDS and STRUCTURES

www.elsevier.com/locate/ijsolstr

Limitations of the Coulomb friction assumption in fretting fatigue analysis

Sam Naboulsi *, Ted Nicholas [1]

Department of Aeronautics and Astronautics, Air Force Institute of Technology (AFIT/ENY), 2950 P St. Bldg 640ENY, Wright-Patterson Air Force Base, OH 45433-7765, USA

Received 28 September 2002; received in revised form 22 January 2003

Abstract

A significant factor in the fretting process, both experimentally and analytically, is the Coulomb friction. Most analyses of fretting fatigue consider a constant coefficient of friction (CCOF) in modeling a contact geometry. This work reevaluates the constant assumption of the Coulomb friction coefficient, and develops a Coulomb friction model based on a non-classical model allowing the coefficient of friction (COF) to be a function of local contact pressure and local slip magnitude. Here, the Coulomb COF varies locally along the contact surface. Results of computations using this model are applied to fretting fatigue experiments utilizing several specific contact geometries, which have nominally identical fatigue lives experimentally. The analysis shows that certain combinations of parameters in the variable coefficient of friction model can produce nominally identical stress states. Such results cannot be obtained using a CCOF.

Published by Elsevier Ltd.

1. Introduction

In 1781, the French engineer C.A. Coulomb published his "Theory des Machines Simples" in which he published the well-known Coulomb law of friction. The classical Coulomb law of static dry friction asserts that relative sliding between two bodies in contact along plane surfaces will occur when the net shear force parallel to the plane reaches a critical value proportional to the net normal force pressing the two bodies together where the constant of proportionality is the coefficient of friction (COF). Physically, Coulomb's law is capable of describing only frictional effects between effectively rigid bodies and gross sliding of one body relative to another. Only the total contact forces and total frictional force are considered, without bothering about how these forces are actually distributed on the contact surface. Hertz in the 1880s successfully solved a static contact problem in elasticity assuming the contact bodies as an elastic half-space with small deformation and an elliptical small contacting area. Using Coulomb's law in a contact problem,

* Corresponding author. Tel.: +1-937-255-6565; fax: +1-937-427-3369.
E-mail address: samir.naboulsi@afit.edu (S. Naboulsi).
[1] Visiting Research Professor from University of Dayton Research Institute, Dayton, OH 45469-0120, USA.

0020-7683/$ - see front matter Published by Elsevier Ltd.
doi:10.1016/S0020-7683(03)00401-3

Duvaut and Lions (1976) and Duvaut (1980) showed that if Coulomb's law is applied pointwise in contact problems involving linear elastic bodies, then the contact stress developed normal to the contact surface is ill defined, except for some very special cases. The elasticity approach to the contact problem is restrictive and can be applied to special problems. The solutions of various complex contact problems have been obtained using numerical methods. The finite element method has been most widely used (e.g. Oden, 1972; Bathe, 1976; Zienkiewicz, 1977; Hughes, 1987, etc.). There are several aspects of actual friction phenomena between metallic bodies that suggest alternative friction laws (i.e. limiting the use of Coulomb COF to total/global contact forces), which represent a marked departure from the classical Coulomb formulation for these type of problems. One of these phenomena is fretting fatigue, and frictional modeling of fretting fatigue is the focus of the present study.

Fretting fatigue refers to the degradation of the mechanical properties of material in a region of contact where cyclic tangential loads occur in the presence of normal or clamping loads. Such a process involves cyclic material damage accrual where many mechanical factors affect the degradation process. Included in these are the contact pressure, the slip amplitude at the interface, the COF and the magnitude of the tangential and bulk stresses at the interface. In fretting fatigue, as opposed to wear or galling, the contact region is one where the two bodies experience relative motion only near the edges of contact (''slip'') while the central region remains in full contact, normally referred to as ''stick.'' Of the many variables associated with the phenomenon (Dobromirski, 1994) one parameter, the relative COF between the contacting bodies, has been shown numerically to have a significant influence on the magnitude of the stresses and relative slip displacements in the contact region (Hutson et al., 2001). Experiments have shown that the magnitude of the average COF changes with number of cycles in fretting of titanium against titanium (McVeigh et al., 1999). While no direct measurements have been made of COF in the slip region where relative motions are of the order of only tens of microns, several computational efforts have deduced values by matching results from models to experimentally observed phenomena. In fretting fatigue experiments on a stainless steel material, elastic–plastic finite element modeling using a higher COF, $\mu = 1.5$ was found to better model the experimentally observed extent of local plasticity than using $\mu = 0.5$ or 1.0 (Swalla and Neu, 2001). In another study Goh et al. (2001) found that in crystal plasticity calculations for Ti–6Al–4V fretting fatigue experiment simulations, a value of $\mu = 1.5$ provided the best simulation of the experimentally observed dimensions of the slip regions of the contact. It is to be noted that these values of COF are considerably higher than *average* values generally measured in contact experiments and subsequently used in modeling of contact geometries. For example, Farris et al. (2001), have reported a saturated value of $\mu = 0.5$ after a large number of fretting fatigue cycles in the same titanium alloy. In other fretting fatigue experiments, a saturated value of an average COF $= 0.65$ was obtained using 1 mm flat pads with a blend radius against specimens of identical Ti–6Al–4V (Gallagher, 2001). The saturated value was reached after approximately 1000 cycles where the initial value of COF was about $\mu = 0.25$. In another study McVeigh et al. (1999) analytically modeled the interfacial conditions in nominally flat contacts and obtained good correlation of computations with experimentally observed amounts of interfacial damage in Ti–6Al–4V specimens using an average value of 0.4 for the COF. In the same material, $\mu = 0.33$ has been used in one investigation as an average value for computations of contact stress fields (Namjoshi et al., 2001) while $\mu = 0.3$ has been used in another (Hutson et al., 2001).

In Nicholas et al. (2001), the K solution for a Mode I crack at the edge of the region of contact, where stresses are maximum, was obtained. While the local stress fields were different for two cases of fretting geometries and loads corresponding to the same life of 10^7 cycles, there was also no correlation of the K fields from the two cases compared. From this observation, the possibility that initiation took place at stress levels lower than the final one obtained in the step test procedure in two cases, and that the final stresses were based on a threshold for crack propagation, was eliminated. Based on these many observations, it was decided to investigate the possibility that the COF is not a constant in the region of slip but, rather, that μ may depend on the relative slip amplitude.

2. Friction model

Classical friction laws assume two bodies are at rest or moving together without relative motion until the tangential force F_t reaches a critical value F_c. This is expressed as

$$\begin{aligned} &F_t \leqslant F_c = \mu_s F_n \quad \text{(No slip or relative motion) and} \\ &F_t = F_c = \mu_s F_n \quad \text{(Slip condition)} \end{aligned} \tag{1}$$

Classical frictional laws are deficient in various engineering contact problems. Non-classical frictional laws include non-linear and non-local laws that are suitable for modeling the physics of engineering applications (e.g. Oden, 1972; Nilsson, 1979; Curnier, 1984; Kikuchi and Oden, 1988). Non-classical friction laws assume the relation between F_t and the tangential displacement u_t proportionally related through a stiffness E_f which may change during the analysis as a function of contact pressure, slip rate, or other field variables dictated by the problem. As the frictional force reaches its critical value, the tangential displacement needs to be determined by considering the equilibrium of the entire system. Both classical and non-classical frictional laws in their standard form have difficulty modeling the frictional contact of fretting fatigue experiments, as mentioned earlier in the introduction. The present work focuses on developing a non-linear pointwise model for fretting fatigue applications based on a combination of classical and non-classical laws.

The slip condition (i.e. $\tau_{crit} \leqslant \mu p$, where τ_{crit} is a shear critical value) developed in the present study is specifically chosen for a fretting fatigue application. Along common pad–substrate surfaces, which are defined as a contact pair, the Coulomb COF is assumed to vary along the contact surface as function of slip magnitude, γ, exponentially, see Fig. 1a, and normal pressure, p, in a power law during slip conditions, see Fig. 1b. Its value is bounded between the upper static friction coefficient, μ_s, and lower dynamic friction coefficient, μ_d. Note that, μ_s is the static coefficient of friction (SCOF), which corresponds to a stick condition (i.e. $\tau_{crit} > \mu p$). During a slip condition the surface resistance decreases, which is reflected in a lower shear traction, i.e. lower COF, and it reaches a lower limit equal to the dynamic coefficient of friction (DCOF), μ_d. These bounding values reflect the limits of COF during a stick and slip cycle.

The value of the Coulomb COF along a contact pair is assumed to decrease exponentially with slip magnitude, i.e. e^{γ}, and to increase in a power law as a function of pressure, i.e. p^n, that is, the COF becomes constant for $n = 0$, is a linear function of pressure for $n = 1$, and is a power law in general for $0 < n < 1$, where the COF reaches a limit beyond a specific pressure value. For the case where $1 < n < +\infty$, the COF becomes unbounded for a given pressure. Further, in the present model, the shear becomes a non-linear

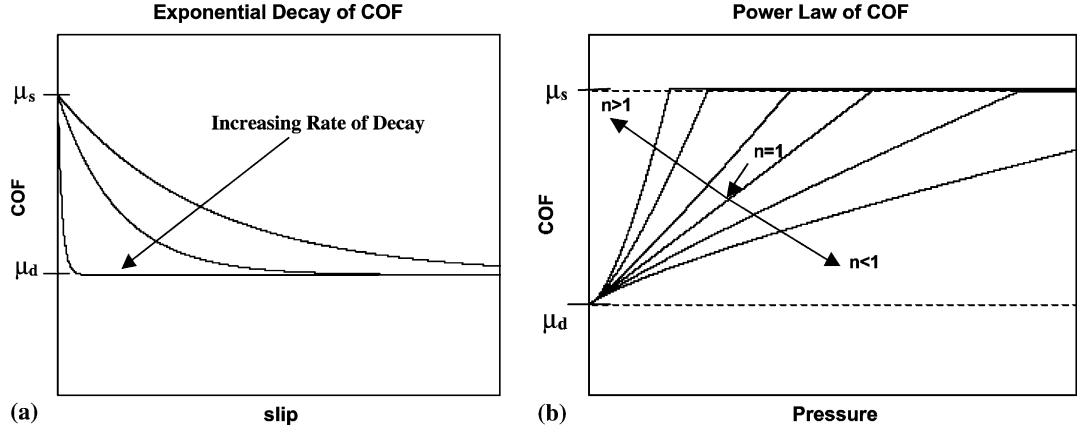

Fig. 1. Variation of COF versus (a) slip in an exponentially function and (b) pressure in a power law function.

function of pressure, except for $n = 0$, where it is a linear function of pressure. Thus, the Coulomb COF, μ, is proportional to slip magnitude and pressure as

$$\mu \propto f(e^{\gamma}, p^{n}), \quad \text{if } \tau_{\text{crit}} \leqslant \mu p \tag{2}$$

or, incrementally the Coulomb COF at an integration point is

$$\mu^{i+1} = \mu^{i} - A(\mu^{i} - \mu_{\text{d}})(1 - e^{-Q\gamma}) + B(\mu_{\text{s}} - \mu^{i})(p^{i+1}/p_0)^{n} H(p_0 - p^{i+1}) \quad \text{and } \mu_{\text{d}} \leqslant \mu^{i+1} \leqslant \mu_{\text{s}} \tag{3}$$

where μ^{i} is the COF at the previous increment, equal to μ_{s} if the contact condition was stick in the previous increment; Q is the rate of exponential decay for the COF during a slip condition (see Fig. 1a); p_0 is the critical normal pressure where, beyond its value, the normal pressure instigates resistance to the slip condition, i.e. increase in COF; $H(p_0 - p)$ is the Heavyside step function which dictates the initiation of slip resistance, i.e. slip resistance starts if the normal pressure, p, exceeds the critical normal pressure, p_0; n is a power law coefficient; and A and B are the proportionality constants to calibrate the effects of slip and stick on COF. The first term in Eq. (3), μ^{i}, is the COF from the previous increment. The second term models the reduction in the COF during slip, which is a function of the slip rate. The third term models resistance to slip or increase in traction along the contact surface due to increase in normal pressure along the contact zone. The relation, $\tau = \mu p$, thus varies along the contact pair, not only with the normal stress, p, but also with the slip rate. The shear stress-based on the Coulomb model is assumed to be

$$\begin{aligned} &\tau^{i+1} = \mu_{\text{s}} p^{i+1} \quad \text{(Stick) and} \\ &\tau^{i+1} = [\mu^{i} - A(\mu^{i} - \mu_{\text{d}})(1 - e^{-Q\gamma}) + B(\mu_{\text{s}} - \mu^{i})(p^{i+1}/p_0)^{n} H(p_0 - p^{i+1})] p^{i+1} \quad \text{(Slip)} \end{aligned} \tag{4}$$

This frictional model can be easily implemented numerically in a finite element code.

3. Numerical modeling

The present investigation specifically focused on frictional modeling in fretting fatigue. Defining interface behavior of contact pairs of the pad–substrate surface based on the frictional model, the finite element method is chosen to solve the problem of fretting of the pad–substrate in contact. The commercial software ABAQUS is used to solve the fretting problem. The frictional model is implemented as a user subroutine, which is an option available in ABAQUS. Three geometric configurations of a flat pad with rounded ends in fretting with a finite width substrate are investigated. Configurations of the pad–substrate are shown in Fig. 2. These configurations are selected to calibrate the fretting fatigue frictional model, since experimental data are available from a previous study (see Hutson et al. (2001) and Nicholas et al. (2001) for experimental apparatus and results).

The frictional model is implemented at integration points of the contact pair if the contact points are determined to be closed where contact pressure is non-zero and compressive. Applying the load incrementally, the relative motion of the contact pair at integration points is determined using equilibrium. Based on the relative displacement, $\Delta\gamma_{\text{r}}$ at the integration points, if rigid sticking, $\Delta\gamma_{\text{r}} = 0$, at the interface occurs, the Lagrange multiplier method is used to enforce a stick condition. Otherwise, a slip condition, $\Delta\gamma_{\text{r}} \neq 0$, occurs. It should be noted that ABAQUS uses the Lagrange multiplier where no relative displacement can occur in the contact stick region. For the slipping condition, the shear stress exceeds the critical stress, and the shear stress at the interface becomes

$$\tau = \tau_{\text{crit}} \tag{5}$$

The radius of all fretting pad's rounded ends is 3.2 mm. The flat width varied in the three configurations, equal to 3.0 mm for the short pad, 6.3 mm for the medium pad, and 19.0 mm for the long pad. The width of all pads is 10 mm, which is also the width of the substrate. The thicknesses of substrates are 2 mm for the

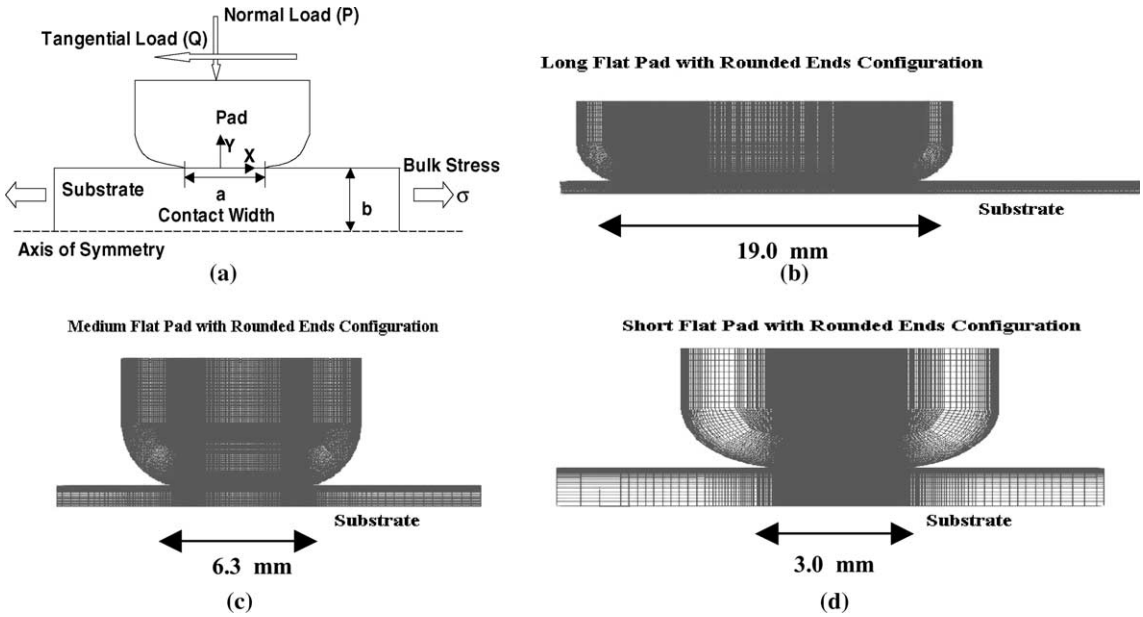

Fig. 2. (a) Geometric configuration of general pad and finite element mesh for the (b) long, (c) medium, and (d) short pad geometries.

short and medium pad, and 4 mm for the long pad, respectively. Both the substrate and pads are made from titanium alloy, Ti–6Al–4V, where Young's modulus is $E = 120$ GPa and Poisson's ratio is $v = 0.3$. Applied normal loads are 21, 21, and 33 kN for the short, medium, and long pad configurations, respectively. The applied bulk stress is 230 MPa for the short pad and 275 MPa for both medium and long pad configurations. This stress corresponds to the experimentally measured bulk stress, which produced a total fatigue life of 10^7 cycles (Hutson et al., 2001; Nicholas et al., 2001).

Finite element meshes for the short, medium, and long pad configurations use two-dimensional, four noded, plane strain quadrilateral elements in the present analyses. Common pad–substrate surfaces are defined as contact pair in ABAQUS. A sliding contact condition is used between the contact pair to transfer loads between the two contacting bodies where the frictional stresses are defined by the fretting fatigue frictional model developed above. Pads are defined as the slave contact surface and substrates are defined as the master contact surface. The contact region consists of stick and micro-slip regions. The stick region does not have any relative movement. The slip region shows a micro-scale relative displacement between the two contact surfaces, and the fretting fatigue frictional model governs the interface's behavior. A variable coefficient of friction (VCOF), μ, is used based on the frictional law defined above.

Refinement of the meshes near the contact zone is crucial to capture the correct stress magnitudes and its distribution. Based on previous studies of fretting fatigue (Hutson et al., 2001; Nicholas et al., 2001) mesh refinement required element sizes ranging between 6 μm to 12 μm to approach a converged solution of contact stresses. The present analysis uses element size of 1.5 μm near the contact zone. For example, the finite element meshes of the short, medium, and long pad are shown in Fig. 2. The meshes for all pad configurations are similar where the contact regions are well refined, specifically near the pad contact edges. In all experiments as well in all analyses, the first step involved the application of the normal load, P, on the fretting pad. Thereafter the fatigue bulk stress, σ_b, was applied to the specimen. After application of the normal load, contact shear stresses develop along the interface due to micro-slip between the two contacting bodies. The shear traction and axial stresses along the contact surface for the finite width substrate for short, medium, and long pads are shown in Fig. 3. These analyses are performed using a constant

Coulomb COF, $\mu = 0.3$. These stresses are validated with published results in Hutson et al. (2001), and they compare favorably. Hence, element refinement of 1.5 μm near contact regions is determined to be sufficient for the present investigation.

Using a constant coefficient of friction (CCOF), $\mu = 0.3$ (Hutson et al., 2001) the stress distribution along the contact surface, which lies parallel to the x-axis, and a close-up look at the stresses near the trailing edge of the short, medium, and long pads are shown in Figs. 3–5, respectively. Note that, in these analyses, the normal stress is slightly positive right near the edge of contact. This clearly represents a lack of accuracy in the computations due to the very high stress gradients in this region. While the mesh might need further refinement, no attempt was made to do this since it is computationally inefficient to reduce the size of the mesh further, which is equal to 1.5 μm in the present analyses. These tensile stresses were not considered in any of the modeling comparisons. Rather, comparisons were made based on maximum stress values (i.e. axial, normal and shear), which varied considerably between the short, medium, and long pads. The percentile difference of the maximum stresses between the three pads (i.e. short and medium, short and long, medium and long) are 23%, 53%, and 39%, respectively, for axial stress, 48%, 72%, and 47%, respectively, for shear stress, and 39%, 63%, and 38%, respectively, for normal stress. It can be seen that the short pad has the highest predicted axial and shear stresses along the contact surface, and the longest pad has the lowest predicted axial and shear stresses. However, upon examination of the computed slip zone for the three pads, which will be shown subsequently, the long pad has the largest slip zone and slip amplitude compared to the medium and short pads, and the short pad has the smallest slip zone and slip amplitude.

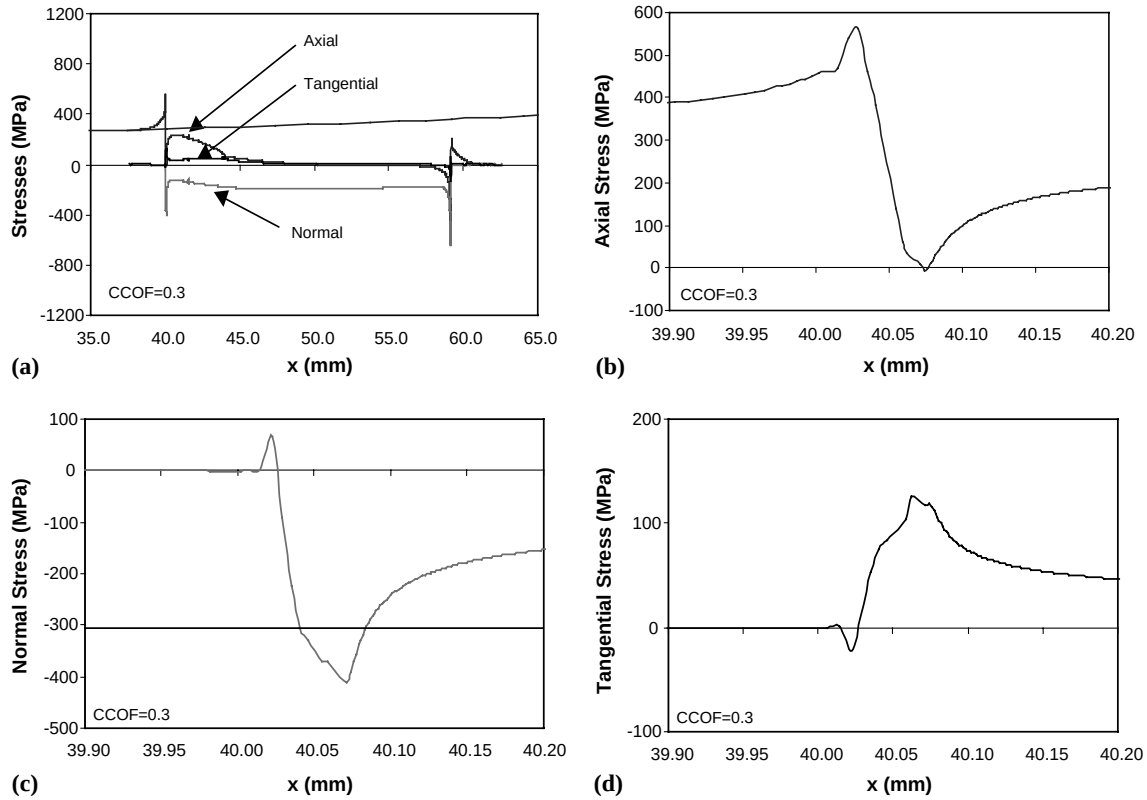

Fig. 3. (a) Stress distribution along the long pad's contact region with constant COF, (b) axial stress at the trailing edge, (c) normal stress at the trailing edge, and (d) tangential stress at the trailing edge.

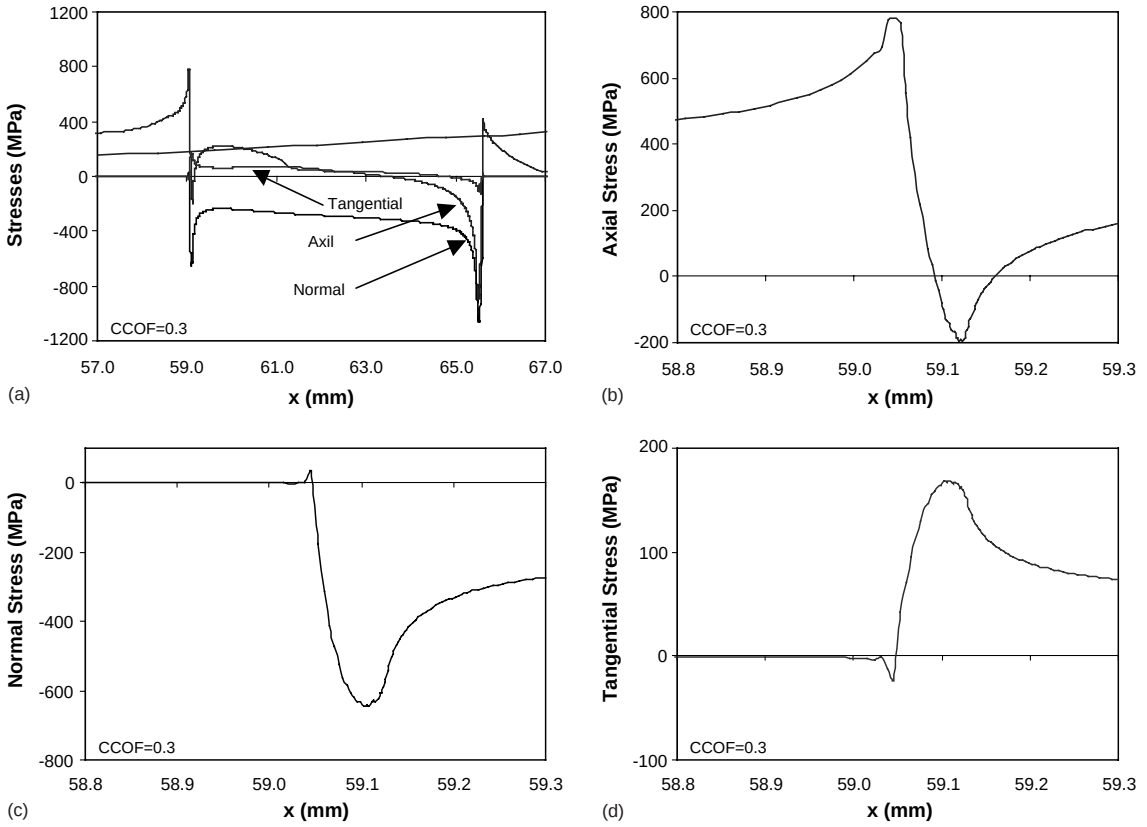

Fig. 4. (a) Stress distribution along the medium pad's contact region with constant COF, (b) axial stress at the trailing edge, (c) normal stress at the trailing edge, and (d) tangential stress at the trailing edge.

This is consistent with the maximum axial stress along the trailing edge where the long pad has the lowest normal stress, and the short pad has the highest normal stress. In Hutson et al. (2001), there have been no slip zone size measurements reported for the experiments modeled. However, based on Hutson (2003), the reason is that the sizes of the scars are too small, on the order of micron, such that accurate measurement is not possible.

It is to be noted here that the numerical simulations are based on values of normal stresses that were applied experimentally and axial stresses (bulk loads) that were obtained experimentally to cause failure in 10^7 cycles. If it is assumed that failure is due primarily to the stress state near the edge of contact where values are maximum, and relative slip does not influence the fatigue initiation and propagation characteristics of the material, then one would expect the three geometries to have nominally similar stress states or maximum stresses to produce nominally identical lives under fretting fatigue conditions. It will be shown later that computed magnitudes of relative slip obtained using larger values of COF are extremely small so that the local conditions look more like pure fatigue than fretting fatigue where damage to the surface is significant.

Hence, based on the above observation, these differences in the computationally predicted maximum contact stress between the three configurations would imply a different cyclic life for those configurations, which also contradicts the reported experimental cyclic life as being nominally identical (10^7 cycles) (Hutson et al., 2001). Thus, either the interfacial modeling of contact surfaces is deficient in representing the

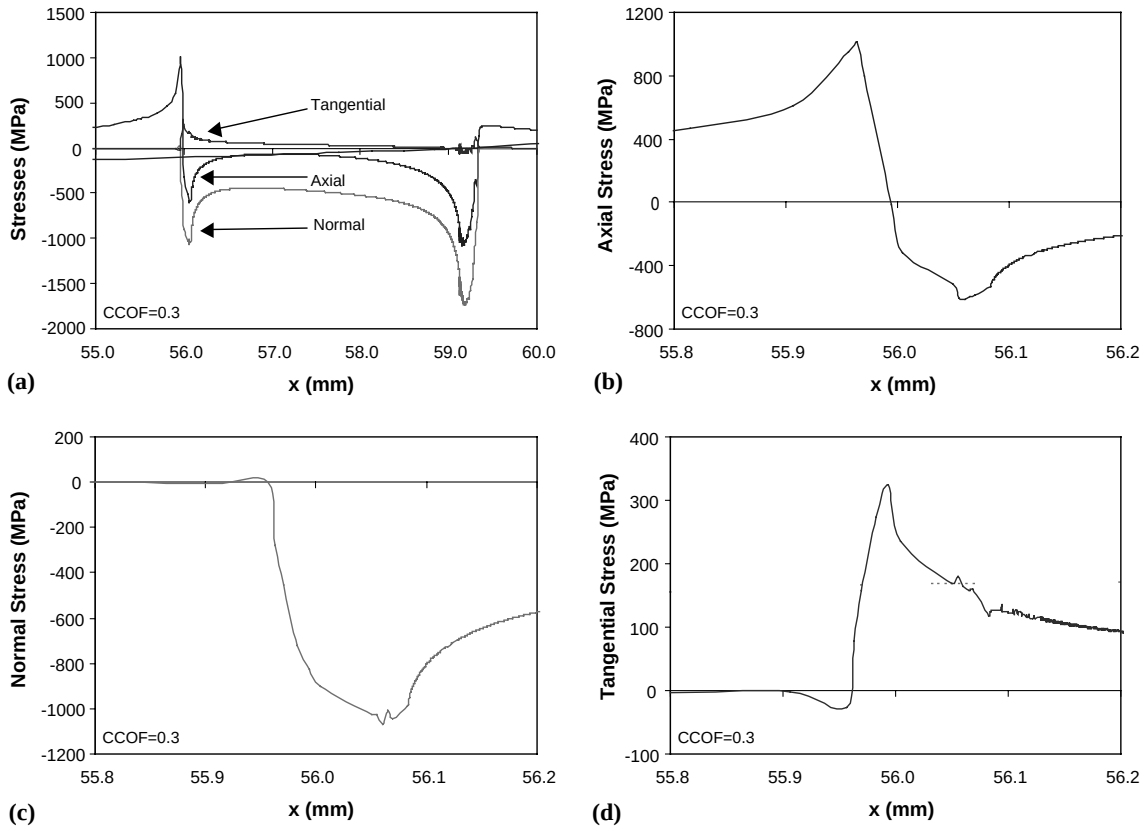

Fig. 5. (a) Stress distribution along the short pad's contact region with constant COF, (b) axial stress at the trailing edge, (c) normal stress at the trailing edge, and (d) tangential stress at the trailing edge.

phenomenological behavior of frictional fretting contact, or crack initiation and growth are independent of the local stress state, which is also unlikely, since damage and fracture mechanics correlate them with the local stress state. Hence, these pad configurations are re-investigated using the variable fretting fatigue frictional model presented earlier.

4. Results and discussion

In a previous study (Hutson et al., 2001) there were large differences between the contact tractions of the long and medium pad–substrate configurations having nominally identical high cycle fatigue lives using the classical friction model with a single value of CCOF. The lack of predicting a similar stress state of geometries and loadings, each of which produced nominally identical high cycle fatigue lives, led to the idea of exploring other values of COF, both constant and variable. It was noticed that slip amplitudes were quite different in the three pad configurations when computed using CCOF. This implies perhaps that a CCOF in fretting fatigue problems might not be as physically realistic as a variable non-classical friction model along contact regions. Hence, the VCOF will be investigated. Then, the results of these analyses will be compared with their counter parts assuming CCOF. Finally a parametric study, which varies the COF in order to

predict a similar stress state of pad–substrate configurations with nominally identical high cycle fretting fatigue lives, will be conducted. The results are detailed below.

In the present study, it is assumed that fretting fatigue life prediction criteria are predicated on contact stress state. For example, in a critical plane stress criterion (e.g. Szolwinski and Farris, 1996; Naboulsi and Mall, 2002), the crack is assumed to initiate along the plane with the maximum value of some stress-based parameter. Other criteria, (e.g. Nicholas et al., 2002; Naboulsi and Mall, 2003), also require the determination of the contact stress field. Hence, considering various pad configurations and load conditions with experimental nominally identical fretting fatigue life, in these cases, it is sufficient to compare their maximum stress. Also, the history dependence of fretting fatigue during cycling causes the stress state to undergo changes (e.g. Naboulsi and Mall, 2002). Such a consideration is beyond the scope of this investigation.

4.1. VCOF analyses

The variable non-classical friction model, presented in Section 2, is used along contact regions of the short, medium, and long pad–substrate configurations. Locally the fretting region consists of a stick region and a slip region with varying slip magnitudes. To better understand the variable frictional model, the analyses of pad–substrate combinations under fretting fatigue assuming a variable non-classical friction model are performed using various values of the constants for the frictional model in Eq. (3) as follows. For the frictional model, proportionality constants A and B are 1.0 and 1.0×10^9, respectively, critical normal stress, p_0, is 1000 GPa, and the exponential and power law coefficients, Q and n, are 1.0×10^5 and 0.01, respectively. Note that the choice of parameters emphasizes the dependence of the COF on the slip magnitude, i.e. the second term in Eq. (3), as compared to pressure dependency, i.e. the third term in Eq. (3). For example, the analyses of the three pads using CCOF are re-analyzed under the same conditions except for using VCOF where SCOF is equal to $\mu_s = 2.0$ and DCOF is equal to $\mu_d = 0.3$. The results are shown in Fig. 6, where the trend of the contact stresses for VCOF show similar characteristics to their counterpart using CCOF. However, using VCOF predicted closer stresses for the three pads than their CCOF counterpart analyses.

A parametric study, where the SCOF and DCOF vary, is performed. In the parametric analyses, the range of SCOF and DCOF is 0.75–2.5 and 0.3–2.0, respectively, which will be stated explicitly for each analysis. The first parametric analysis holds the DCOF constant at 0.3 and varies the SCOF between 0.75 and 2.0. The maximum axial stress distribution at the contact zone for the short, medium, and long pad versus SCOF are shown in Fig. 7a. The results show that the axial stresses increase with higher SCOF, since larger values of SCOF produce a stronger bond at the pad–substrate interface and a higher stress state. However, the differences between the axial stresses for the three pads decrease with increasing SCOF, which will be examined in detail later. Similarly, the shear stress for the three pads as a function of the SCOF is shown in Fig. 7b. The results show that the difference in the maximum shear stress is lowest at SCOF equal to $\mu_s = 1.5$. Furthermore, the size of the slip zone and the maximum slip amplitude versus SCOF are plotted in Fig. 8. The results show that the size of the slip zone decreases as the SCOF increases as expected. Their values for the three pads seem to converge toward an equivalent single size as the SCOF value increases. Fig. 8 also shows that the size of the slip zone for the three pads are in the tens of micron range or lower except for the long pad where the size of the slip zone becomes thousands of microns at SCOF equal to $\mu_s = 1$, and the analysis did not converge for SCOF less than one, i.e. $\mu_s < 1$. This is consistent with experimental observation (Hutson et al., 2001) where the long pad showed larger scar sizes in comparison to the medium and the short pads.

Similarly, the second parametric analysis varied the DCOF, where also the SCOF varied in order to maintain a reasonable spread between the COFs lower bound, DCOF, and upper bound, SCOF. Hence, in this case the SCOF ranged between 0.75 and 2.0, while the SCOF ranged between 1.0 and 2.5. The maximum axial and shear stresses are shown in Fig. 9a and b, respectively. The results show similar trends

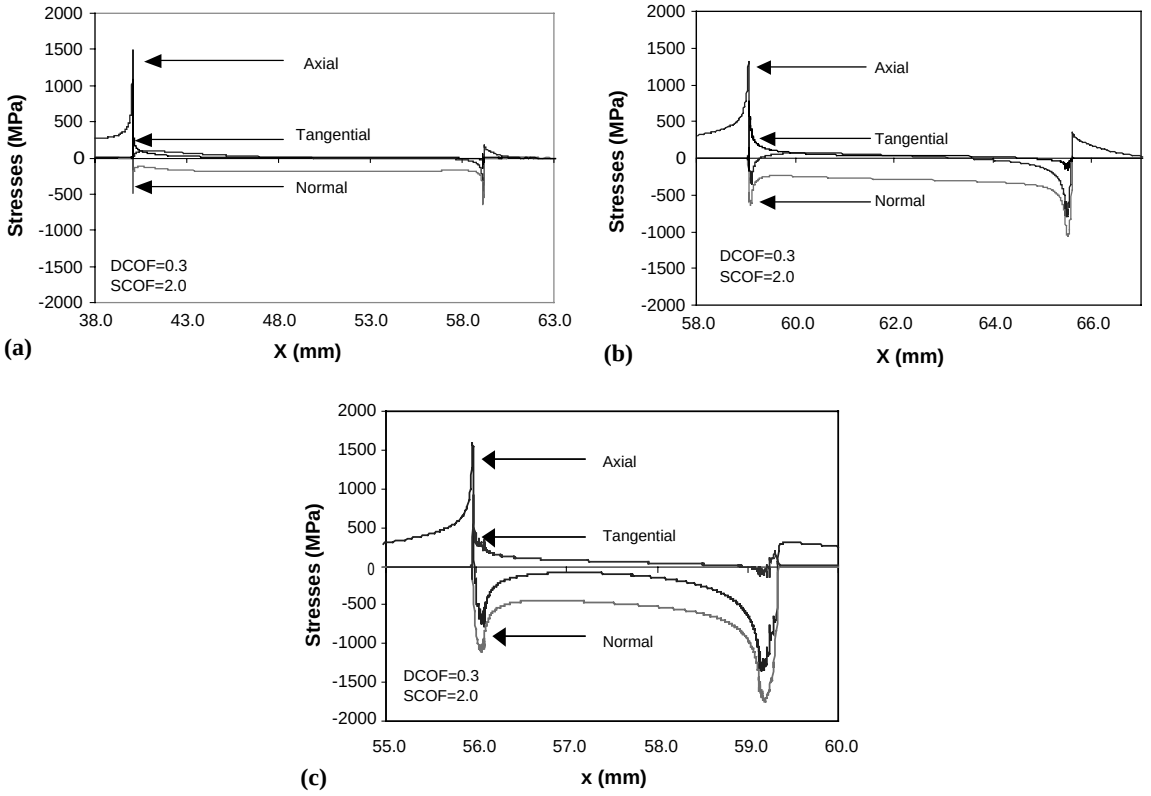

Fig. 6. Stress distribution along the contact regions with variable COF, where SCOF is $\mu_s = 2.0$ and DCOF is $\mu_d = 0.3$, for (a) long, (b) medium, and (c) short pads.

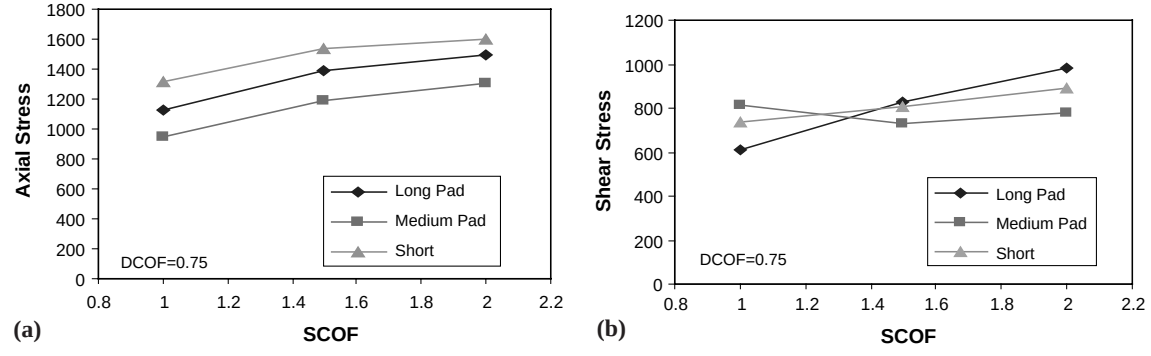

Fig. 7. Maximum stress along contact region for the three pads versus SCOF, μ_s, and fixed DCOF equal to $\mu_d = 0.75$ for (a) axial stress and (b) shear stress.

to the previous case where the SCOF is varied and DCOF is held constant. However, in this case the axial stress showed sharp changes as both the SCOF and DCOF are varied at lower values (e.g. from $\mu_s = 1.0$ and $\mu_d = 0.75$ to $\mu_s = 2.0$ and $\mu_d = 1.0$). The size of the slip zone versus the DCOF is also plotted in Fig. 9c. It shows a similar trend to the previous case where the sizes of the slip zone for the three pads seem to

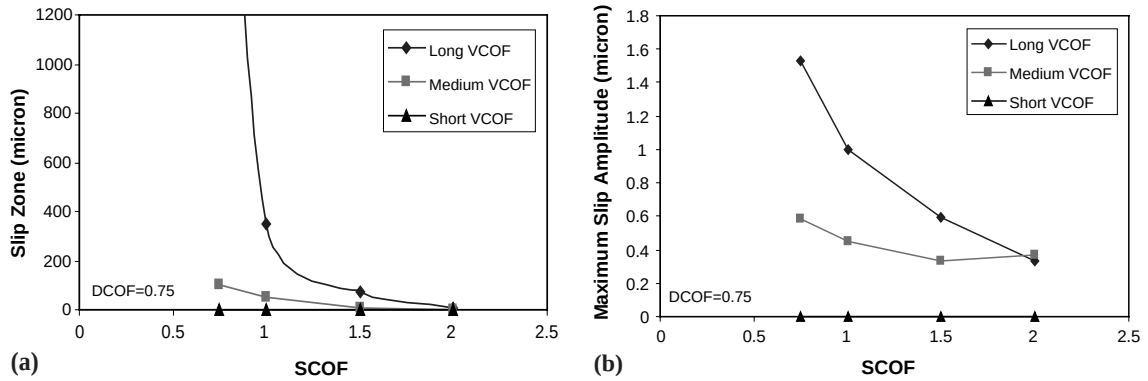

Fig. 8. SCOF versus (a) slip zone and (b) maximum slip amplitude for the short, medium, and long pads where fixed DCOF equal to $\mu_d = 0.75$ is used.

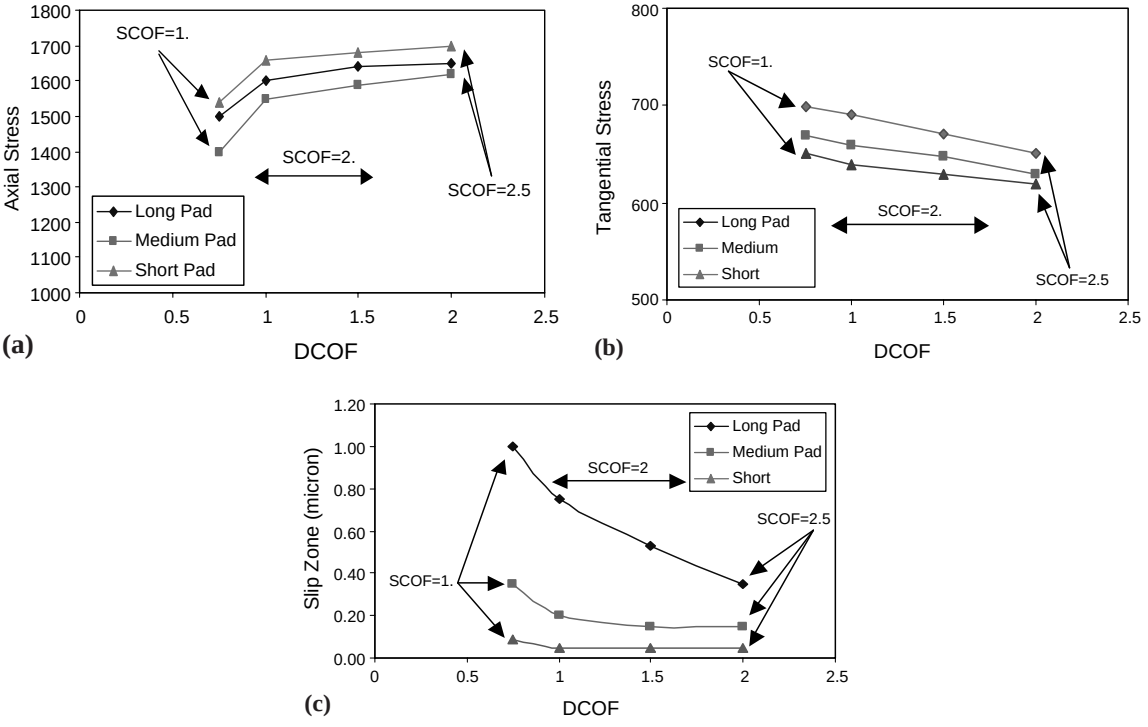

Fig. 9. DCOF, μ_d, versus (a) maximum axial stress along contact regions, (b) maximum tangential stress along contact regions, and (c) size of the slip zone for the short, medium, and long pads where various SCOF values, μ_s, are used.

converge toward an equivalent single size as the DCOF increases. However, the actual sizes of the slip zone are smaller and they range in a fraction of a micron. That is, the analyses indicate a large stick zone, especially as the COF increases (e.g. SCOF, $\mu_s > 2.5$ and DCOF, $\mu_d > 2.0$).

The percentile difference of the stresses between the three pads is investigated for various COF values, since the maximum stress value depends on the choice of both SCOF and DCOF. Their values for the

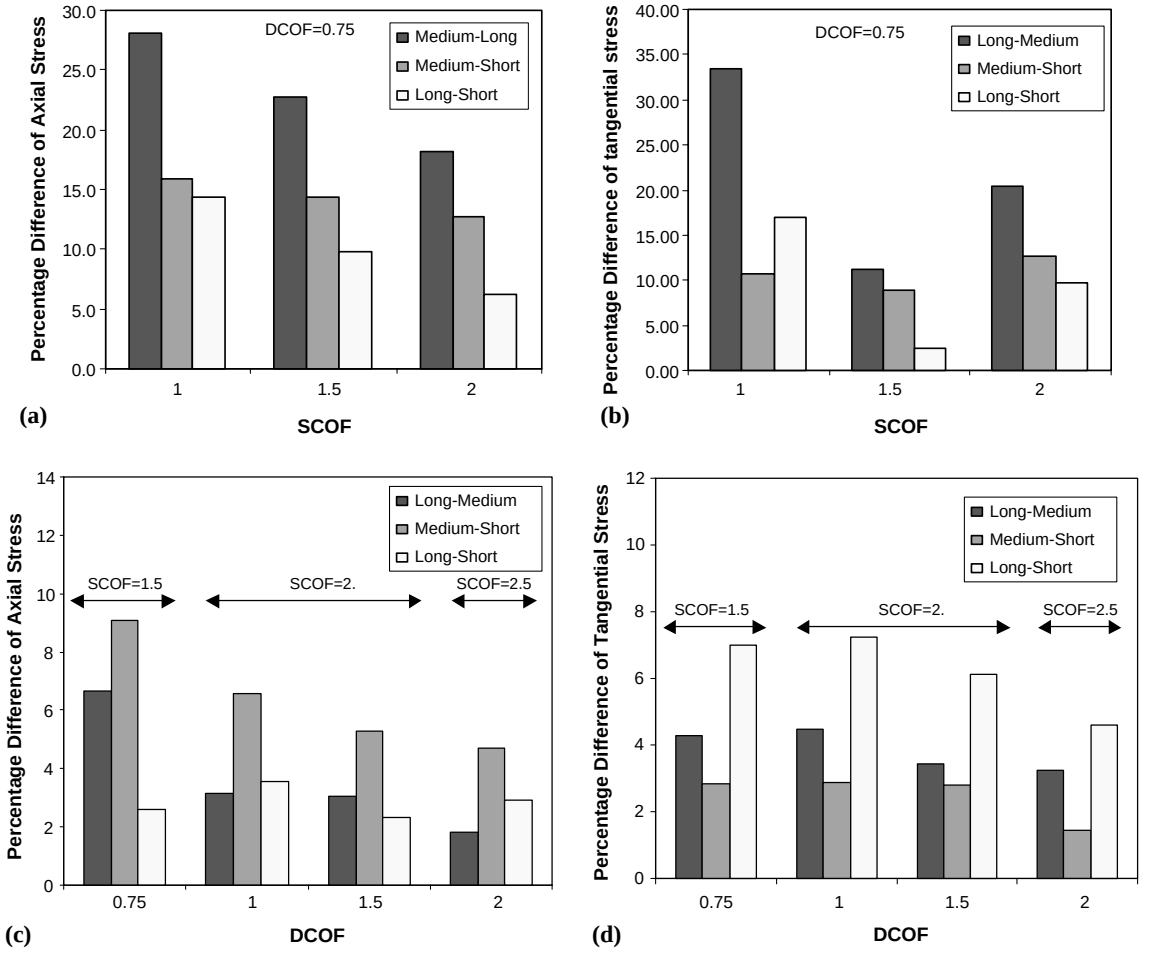

Fig. 10. Percentage difference between the three pads of (a) axial stress versus SCOF with fixed DCOF, (b) shear stress versus SCOF with fixed DCOF, (c) axial stress versus DCOF with various SCOF, and (d) shear stress versus DCOF with various SCOF.

maximum axial and shear stresses are plotted versus COF in Fig. 10. They mainly show that the least percentile difference occurred at large values of SCOF and DCOF where the size of the slip zone is very small and approaches a pure stick condition. For example, the percentile difference of the axial stress versus the SCOF, shown in Fig. 10a, indicates that it decreases as the SCOF increases. However, for the results shown in Fig. 10b, the least percentile difference occurred at SCOF equal to $\mu_s = 1.5$. The percentile differences of both stresses in general are in the double digit. Similarly, the percentile differences of the axial and shear stresses versus the DCOF are plotted in Fig. 10c and d, and they show similar trends. However, their percentile values are in the single digit range and they are less sensitive to the variation of DCOF.

4.2. VCOF versus CCOF analyses

A comparison between the analyses obtained from the widely used CCOF approach and the present VCOF model is performed. Comparisons of the maximum axial and shear stresses as function of COF are shown in Fig. 11a for CCOF and VCOF. Similarly, a comparison of the size of the slip zone and the

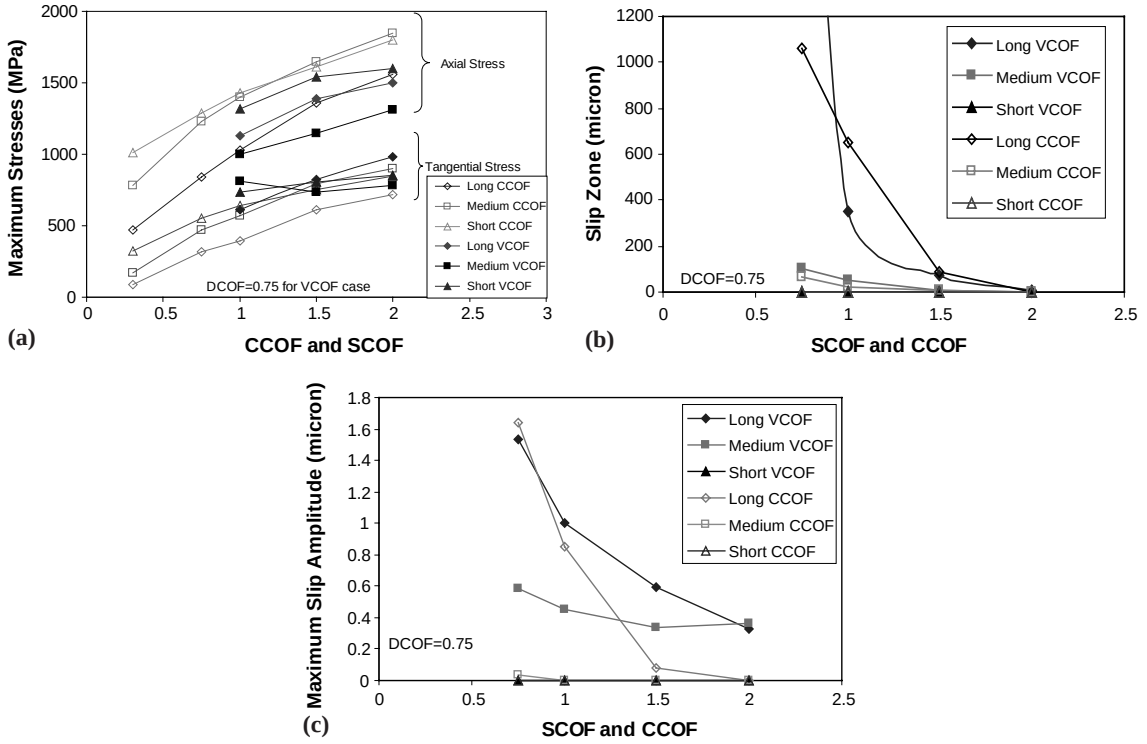

Fig. 11. Comparison of SCOF and CCOF versus (a) maximum axial stress, (b) slip zone, and (c) maximum slip amplitude.

maximum slip amplitude are shown in Fig. 11b and c. In general the trends of the maximum stresses and size of the slip zone are similar as a function of the CCOF and VCOF.

The maximum value for the axial and shear stresses is higher with higher CCOF and VCOF, and the size of the slip zone is lower with higher values of CCOF and VCOF. However, considering the trend with respect to the three pad configurations (long, medium, and short) in the CCOF cases, the maximum stress for the short pad is the highest, and for the long pad is the lowest. On the other hand, for the VCOF cases, the stresses at the contact are implicitly a function of slip, since the COF is assumed to be a function of slip as seen in Eq. (3). This, in general, leads to lower axial stresses due to lower COF during slip. The size of the slip zone with respect to the three pad configurations is the largest for the long pad and the smallest for the short pad, which decreases as the CCOF and VCOF increase. The short pad showed an almost complete stick condition for both CCOF and VCOF, while the long pad showed a large slip zone. For example, for the long pad, the use of a small value of COF, $\mu = 0.5$, produced, in general, unrealistic values of slip amplitude and unbounded slip zone size (i.e. gross slipping condition) in the VCOF case. They also show that CCOF analyses lead to a smaller slip zone and maximum slip amplitude when compared to VCOF analyses. For example, an almost complete stick condition occurred at CCOF, $\mu \geqslant 1.5$ for medium and long pads. However, results from VCOF showed lesser stick conditions, which start to dominate at SCOF $\mu_s > 2.0$.

Of significance is the observation that the percentile difference of maximum axial and shear stresses between the three pads as function of CCOF and VCOF are comparable. The percentile differences are shown in Fig. 10 for the VCOF and Fig. 12 for the CCOF. Their trends as function of COF are similar, whereas the percentile difference is reduced as the CCOF and VCOF increases. In general, the

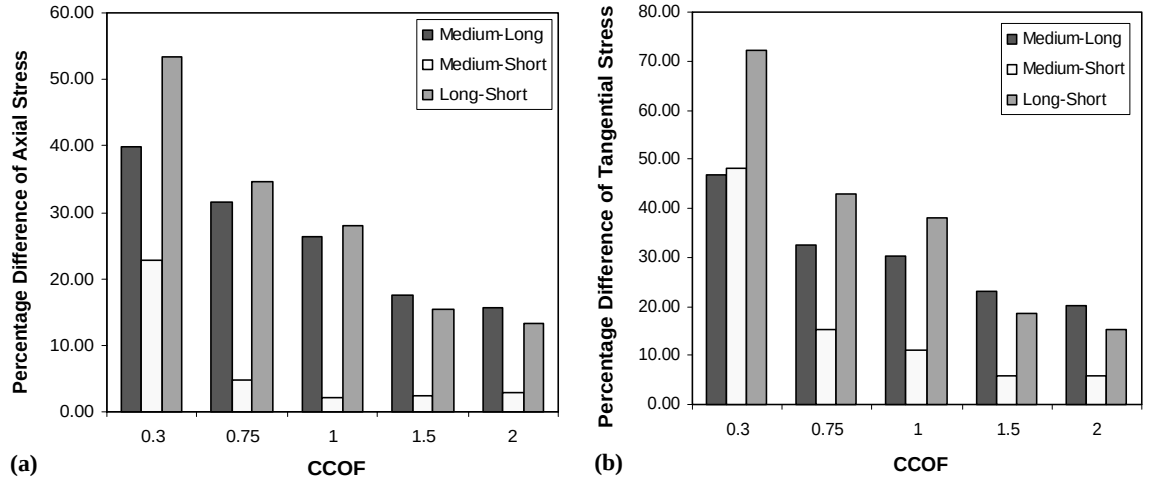

Fig. 12. The three pad's CCOF versus (a) percentage difference of maximum axial stress and (b) percentage difference of maximum shear stress.

comparison of the percentile difference of VCOF in Fig. 10 and CCOF in Fig. 12 shows higher percentile differences of maximum stresses from CCOF analyses than their counterpart obtained from VCOF. However, it becomes less significant as larger values of COF are used in the analyses. That is, for the present analyses, it becomes less significant when the COF is in the range of $1.0 \leqslant \mu \leqslant 2.0$. While one expects even less difference as $\mu \geqslant 2.0$, however, for such COF values a stick condition dominates the analysis and might be physically questionable for fretting fatigue since by definition slip must exist even at a very localized region.

4.3. Nominally identical life predictions of various pad configurations

The comparisons made in the previous sections are aimed at finding stress fields that are nominally identical because the boundary conditions and applied loads on each pad were found to produce the same fatigue life of 10^7 cycles experimentally. If a given fatigue life is obtained from several different geometric and loading conditions, it is expected that the stress state is similar in each of the conditions. Only differences in the slip conditions, primarily the magnitude of relative slip, could account for different stress states because of possible differences in the surface damage caused during the cyclic slip process. The analytical results obtained here depend on only one unknown parameter to fully describe the contact conditions, namely the COF. The numerical results show that the best matching of stress states is obtained when the COF tends towards higher numbers in the range of 1.0–2.0. Under these high values of COF, the size of the slip zone and the magnitude of relative slip become extremely small. As the amount of relative slip decreases, the conditions in the contact region become closer to those of pure fatigue than fretting fatigue because changes to the surface condition due to relative motion of contacting surfaces become negligible. The local contact stress peaks, on the other hand, do not disappear, so fatigue still occurs due to cyclic stresses of fairly large amplitudes. The matching of stress states from the different contact conditions now becomes the only criterion for deducing the nature of the COF. The results obtained herein then point towards a high value of COF and an inference that a VCOF, dependent on slip amplitude, may be the best way to match stress states from the three experimental configurations.

5. Conclusions

Constitutive modeling of frictional phenomena as a pointwise non-classical non-linear law where the COF varies non-linearly with slip rate and normal pressure shows promising results. A fretting frictional model with VCOF, implemented to reinvestigate the fretting fatigue of three contact geometries, produced results that show the stress state at the trailing edge of contact varies with the choice of COF. Based on the cases analyzed, a higher COF ($1.0 \leqslant \mu \leqslant 2.0$) produced the best match of stress states for the three configurations, which had identical fretting fatigue lives. Better performance of the frictional model than had been expected by using these higher values for COF is consistent with other studies finding similarly high values of COF. Analyses of other cases are required to further test the frictional model capabilities in predicting phenomenological behavior of friction under fretting fatigue conditions.

Analyses of long, medium, and short pad configurations, where the (variable) COF is bounded between a lower limit, $\mu_d = 1.0$, and an upper limit, $\mu_s = 2.0$, were performed. The results showed similar results for maximum stresses for the three configurations. These nominally similar results, combined with computations of slip magnitudes that are small enough to eliminate the probability of surface wear having an effect on the material behavior in fatigue, lead one to speculate that values of COF are much higher locally than those reported as average values. Further, the VCOF assumption appears to produce more consistent results than a CCOF model, although the differences here are not as significant, which is attributed to the small slip zone. It is also observed that for the long pad, the use of a small value of COF, $\mu = 0.5$, produced, in general, unrealistic values of slip amplitude and slip zone size with either a CCOF or VCOF model. Finally, the investigation of COF shows promising results in better predicting the stress state of various pad geometries that produce nominally identical fretting fatigue lives. However, the present investigation needs to be extended to include additional pad geometries under various conditions (e.g. experiments with larger slip zones).

References

ABAQUS. Standard User's Manual, Hibbit, Karlsson and Sorensen, Inc., Pawtucket, RI.

Bathe, K.J., 1976. Finite Element Procedures in Engineering Analysis. Prentice-Hall, Englewood Cliffs.

Curnier, A., 1984. A theory of friction. Int. J. Solids Struct. 20, 637–647.

Dobromirski, J.M., 1994. Variables of fretting processes: are there 50 of them? In: Waterhouse, R.B., Lindley, T.C. (Eds.), Fretting Fatigue, ESIS 18. Mechanical Engineering Publications, London, pp. 60–66.

Duvaut, G., 1980. Problemes Mathematiques de la Mecanique-Equilibre d' an Solide elastique Avec Contact Unilateral et Frottement de Coulomb. C.R. Acad. Sci. Paris 290 (Serie A), 263–265.

Duvaut, G., Lions, J.L., 1976. Inequalities in Mechanics and Physics. Springer Verlag, Berlin.

Farris, T.N., Murthy, H., Perez-Ruberte, E., Rajeev, P.T., 2001. Experimental characterization of fretting fatigue of engine alloys. In: Proceedings of the 6th National Turbine Engine High Cycle Fatigue Conference, Jacksonville.

Gallagher, J.P., (Ed.), 2001. Improved High Cycle Fatigue (HCF) Life Prediction, Final Report, Contract F33615-96C-5269, University of Dayton Research Institute, AFRL-ML-WP-TR-2001-4159.

Goh, C.-H., Wallace, J.M., Neu, R.W., McDowell, D.L., 2001. Polycrystal plasticity simulations of fretting fatigue. Int. J. Fatigue 23, S423–S435.

Hughes, T.J.R., 1987. The Finite Element Method—Linear Static and Dynamic Finite Element Analysis. Prentice-Hall, Englewood Cliffs.

Hutson, A.L., 2003. Private communication.

Hutson, A.L., Nicholas, T., Olson, S.E., Ashbaugh, N.E., 2001. Effect of sample thickness on local contact behavior in a flat-on-flat fretting fatigue apparatus. Int. J. Fatigue 23 (Supp. 1), 445–453.

Kikuchi, N., Oden, J.T., 1988. Contact Problem in Elasticity: A Study of Variational Inequalities and Finite Element Methods. SIAM Publication, Philadelphia.

McVeigh, P.A., Harish, G., Farris, T.N., Szolwinski, M.P., 1999. Modeling contact conditions in nominally-flat contacts for application to fretting fatigue of turbine engine components. Int. J. Fatigue 21, S157–S165.

Naboulsi, S., Mall, S., 2002. Investigation of high cycle and low cycle fatigue interaction on fretting behavior. Int. J. Mech. Sci. 44, 1625–1645.

Naboulsi, S., Mall, S., 2003. Fretting fatigue crack initiation behavior using process volume approach and finite element. Tribol. Int. 36, 121–131.

Namjoshi, S.A., Jain, V.K., Mall, S., 2001. Improved fretting-fatigue behavior of Ti–6Al–4V by shot-peening. In: Proceedings of the 6th National Turbine Engine High Cycle Fatigue Conference, Jacksonville.

Nicholas, T., Hutson, A.L., Olson, S., Ashbaugh, N., 2001. In search of a parameter for fretting fatigue, advances in fracture research. In: Ravi-Chandar, K., Karihaloo, B.L., Kishi, T., Ritchie, R.O., Yokobori Jr., A.T., Yokobori, T. (Eds.), Proceedings of ICF-10. Elsevier. Paper # 0809, CD ROM.

Nicholas, T., Hutson, A., John, R., Olson, S.A., 2002. Fracture mechanics methodology assessment for fretting fatigue. Int. J. Fatigue, in press.

Nilsson, L., 1979. Impact loading on concrete structures. Publication 79:1, Chalmers University of Technology, Gothenburg.

Oden, J.T., 1972. Finite Element of Nonlinear Continua. McGraw-Hill, New York.

Swalla, D.R., Neu, R.W., 2001. Influence of coefficient of friction on fretting fatigue crack nucleation prediction. Tribol. Int. 34, 493–503.

Szolwinski, M., Farris, T., 1996. Mechanics of fretting fatigue crack formation. Wear 198, 93–107.

Zienkiewicz, O.C., 1977. The Finite Element Method. McGraw Hill, London.